

East Tennessee State University

Digital Commons @ East Tennessee State University

Undergraduate Honors Theses

Student Works

5-2020

The Effects of Total Body Proton Irradiation on Mouse Myometrium

Lillith Bulawa

Follow this and additional works at: <https://dc.etsu.edu/honors>



Part of the [Obstetrics and Gynecology Commons](#), [Other Animal Sciences Commons](#), [Radiation Medicine Commons](#), and the [Reproductive and Urinary Physiology Commons](#)

Recommended Citation

Bulawa, Lillith, "The Effects of Total Body Proton Irradiation on Mouse Myometrium" (2020). *Undergraduate Honors Theses*. Paper 548. <https://dc.etsu.edu/honors/548>

This Honors Thesis - Withheld is brought to you for free and open access by the Student Works at Digital Commons @ East Tennessee State University. It has been accepted for inclusion in Undergraduate Honors Theses by an authorized administrator of Digital Commons @ East Tennessee State University. For more information, please contact digilib@etsu.edu.

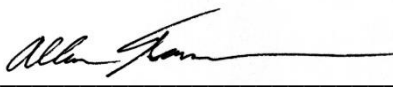
The Effects of Total Body Proton Irradiation on Mouse Myometrium

Lillith Bulawa

April 22, 2020

An Undergraduate Thesis Submitted in Partial Fulfillment
of the Requirements for the
University Honors Scholars Program
Honors College
and the
College of Public Health
East Tennessee State University

Lillith Bulawa, Author Date

 4/20/20

Dr. Allan Forsman, Faculty Mentor Date

 4/20/20

Dr. Michelle Chandley, Faculty Reader Date

Table of Contents

Abstract	3
Introduction	4
Materials & Methods	10
Results	14
Discussion	30
Limitations	31
Conclusion	31
References	32
Appendix	35

Abstract

The boundaries of human space exploration continue to expand with new technology and discoveries making it even more important to investigate the effects of space on biological systems. Although humans have explored space in small increments, reproductive studies must be conducted to determine if stable short- or long-term residences for humans can exist in space. This study explored the effects of whole-body proton radiation on uterine smooth muscle known as the myometrium. Two types of mice utilized in this study were C57BL/6 and B6.129S6Cybb^{tm1Din/J} NOX2 knockout mice. C57BL/6 mice are standard laboratory mice that were used to represent the wildtype treatment group (N=18). The B6.129S6Cybb^{tm1Din/J} NOX2 knockout mice have the NADPH Oxidase 2 gene shut off and represented the NOX2 Knockout treatment group (N=18). A third treatment group was made up of half of the C57BL/6 mice and were fed apocynin (N=18). Apocynin has been shown to inhibit NADPH oxidase production in mice. NADPH Oxidase 2 is involved in the production of deleterious Reactive Oxygen Species (ROS); thus, apocynin should reduce the production of ROS in mice exposed to radiation. Different doses of radiation (0Gy, 0.5Gy, and 2.0Gy) were applied to the myometrium creating three different treatment subgroups within each mouse strain. The mice received 250 MeV protons at an approximate dose rate of 70cGy/ minute. Myometrium tissue was obtained one week following the radiation treatment. The uteri were removed, embedded, sectioned, and stained in hematoxylin and eosin solution. Thickness was determined by taking five measurements each of the outer longitudinal layer length, the inner circular layer length and the total length of both layers of the myometrium for three individual pieces of tissue for each animal. A one-way analysis of variance (ANOVA) was used to determine statistical differences between the groups and subgroups. Wildtype control mice exposed to 2.0Gy (N=5) of radiation had the thickest outer longitudinal layers compared to wildtype mice exposed to 0Gy (N=5) and 0.5Gy (N=6) ($p=0.005$, $p=0$). In the apocynin fed and Knockout treatment groups, the subgroups exposed to 0Gy had the thickest layers compared to their respective subgroups exposed to 0.5Gy and 2.0Gy. The apocynin fed mice exposed to 0Gy (N=6) outer longitudinal layer was statistically significantly thicker than the apocynin-fed mice exposed to 0.5Gy ($p=0.004$; N=6). The inner circular layer of the apocynin-fed mice exposed to 0.5Gy was statistically significantly thicker than the apocynin-fed mice exposed to 2.0Gy ($p=0.001$; N=6). Amongst the treatment groups, the wildtype control versus the apocynin fed mice exposed to 0Gy showed the apocynin-fed group to have the thicker outer longitudinal layer ($p=0.003$) and combined layers ($p=0.001$). Overall, the knockout group showed no statistical difference when compared to the wildtype control group. Further studies are necessary to reduce the possible confounding effect of the estrous cycle in the mice. The different phases of the mice estrus cycle may inadvertently affect the mouse uterine thickness due to the fluctuations in hormones. This study will add to the limited research regarding the female reproductive system in hopes of expanding the knowledge needed to actualize space colonization.

Introduction

An integral part of colonizing any foreign land is ensuring the land is viable as a long-term option. Stable colonies need to be able to increase their population over time, making the health and fertility of women a priority. It is already well established that space affects the human body negatively in many ways. For instance, astronauts undergo changes to their physiology that mimic aging such as cardiovascular deconditioning, a reduction in bone density, and muscle atrophy. The major contributing factors for these adaptations to the human body are the microgravity environment and constant radiation in space (Demontis et al, 2017). The effects of whole-body radiation on the myometrium of the uterus will be the focus of these studies.

The human female uterus can be divided into the fundus region, the main body (or corpus), and the cervix. The fundus is the most superior part of the uterus and is connected to the uterine tubes. The main body is where the embryo will implant and gestate. Finally, the cervix is the muscular circular tissue that will dilate to allow the fetus to pass into the birth canal. Mice have bicornate uteri while human uteri are pyriform shaped. In other words, mice uteri have two uterine horns that meet at the uterine body while humans have a smooth pear-shaped uterus without discernible horns. The uterine wall, of humans, is comprised of three layers; the endometrium, myometrium, and perimetrium. When a placenta forms to provide life support to the embryo, it attaches to the innermost layer, the endometrium. During human menstruation the endometrium, which is two layers, is shed. The two layers are the stratum functionalis and the stratum basalis and it is the former which is shed while the latter remains relatively constant (Baerwald, 2004). In mice, the endometrium is composed of luminal epithelium and glandular epithelium embedded in stromal tissue and myometrium (Boretto, 2017). Animals which exhibit estrus cycles rather than menstrual cycles are either monestrous or polyestrous. A monestrous animal, such as a dog, will

have one long estrous cycle per year followed by anestrous. Mice, which are polyestrous have continuous cycles. The endometrial layer in monestrous animals are subject to more changes than polyestrous animals (Handlin, 2000). That is not to say that the mice endometrium does not change; the endometrial layer expands during proestrus and estrous (Boretto, 2017).

The myometrium is the middle layer of the uterus, the main function of which is to produce uterine contractions. During labor, the smooth muscle contracts to force out the newborn, followed by the placenta. The mouse myometrium is double layered while the human myometrium is formed from three layers (Escalante, 2017). If damaged or weakened it can result in uterine rupture. Uterine rupture is a condition where the myometrium completely separates and is a life-threatening condition. The female can have severe hemorrhaging, placenta abruption, or the amniotic sac and fetal parts may get pushed through the tear (Hawkins et al, 2018). The perimetrium is the outermost layer of the uterus, covering it entirely. Many studies regarding function of the female reproductive tract following irradiation utilize data from women that have been previously exposed to radiation either from nuclear accidents or cancer treatments. Animal models where the uterus of the animal was exposed to radiation were performed to study the damaging effects on the tissues. Mice have commonly been used to simulate the damage incurred by spaceflight on the human body as well as models to ethically study reproduction.

The estrous phase of the mouse can act as a confounding factor during female reproductive studies. After reaching sexual maturity, physiological changes due to reproductive hormones occur that are dependent on the estrous phase of the mouse. The mouse estrus cycle consists of four phases: proestrus, estrus, metestrus, and diestrus occur within four to five days. The estrus phase can be determined experimentally by analyzing the cell composition of vaginal smears. Proestrus is characterized by a surge in estrogen followed by a dramatic increase in luteinizing hormone

(LH) and follicular stimulating hormone (FSH). The increase in LH and FSH triggers ovulation. At this point, the vaginal smears will contain predominantly nucleated epithelial cells. Next, estrus occurs, and estrogen levels steadily decline. The cells present are clustered cornified squamous epithelial cells. Metestrus can be identified by low levels of estrogen and a mixture of leukocytes, nucleated epithelial, and cornified squamous epithelial cells. Lastly, diestrus is when estrogen level rise once again and can be identified by the presence of leukocytes in vaginal smears (Caligioni, 2009).

The complication of the mouse estrous cycle can be circumvented by taking advantage of the Lee Boot Effect. In 1956, two scientists, S. Van der Lee and L.M.Boot, discovered that the estrous cycle of mice, or other rodents, could be manipulated (Whitten, 1959). When female mice are housed together away from any males their estrous cycle can be forcibly prolonged in the diestrus stage or altogether suppressed. The estrogen dependent pheromone 2,5-dimethylpyrazine has been thought to cause the arrest of the estrous cycle by reducing luteinizing hormone levels and increasing prolactin levels. The hormone can be found in the uterus of female mice and detected by the vomeronasal organ (Ma et al, 1998). The Lee Boot Effect is useful in mice reproductive studies because it can remove the confounding effects of the estrous cycle.

Very few studies have evaluated the effects of radiation specifically on the uterine myometrium due to ethical constraints. There are, however, case studies of women that underwent radiation for childhood cancers or women that were subjected to radiation from nuclear bombs that can be referenced. A recent review of literature relating to the impacts of uterine radiation on future fertility and pregnancies in humans found that previous irradiation is associated with smaller uteri and increased pregnancy complications. For instance, “exposure of adult uterus to [Total Body Irradiation] (12 Gy) is associated with increased risk of miscarriage, preterm labour, and low birth

weight babies” (Wann Tinn Teh, 2014). It is thought that the radiation causes damage to the endometrium which impairs normal decidualization and implantation of the embryo. The low birth weight may be a consequence of reduced blood flow from damaged uterine vasculature. Preterm labor and delivery may be a result of reduced uterine elasticity and volume caused by myometrial fibrosis. The myometrium is seen to atrophy under direct radiation which can cause uterine rupture. Interestingly, it was found that a combination of pentoxifylline and tocopherol (Vitamin E) was able to ameliorate the effects of radiation by increasing the size of the uterus, endometrial thickness, and uterine vascularization. The patients were given 400mg of pentoxifylline and 500IU of α -tocopherol twice a day for at least 9 months. One of the known functions of Vitamin E is to reduce free radicals such as reactive oxygen species (Wann Tinn Teh, 2014). The reduction of free radicals’ aids in decreasing chromosomal damage.

One case followed the pregnancy of a primigravida woman who had been treated with whole body radiation to treat childhood leukemia. At 17 weeks gestation she experienced uterine rupture and placenta percreta. A primigravida woman is someone who has become pregnant for the first time. Placenta percreta is when the placenta attaches and grows through the uterine wall. The physicians opted to do a hysterectomy. Subsequent examination of the uterus showed the myometrium was between one and six millimeters thick and even absent in some areas (Norwitz, 2001). The whole-body radiation during her childhood cancer treatment was hypothesized to be the cause of the weakened myometrium. According to a longitudinal sonographic study conducted on 25 uncomplicated pregnancies, an average myometrial thickness of a woman 17 weeks pregnant should be around 11mm (Degani, 1998). The leukemia patient clearly had an abnormal myometrium.

Many studies relating to the effects of radiation on human physiology were conducted on the survivors of the atomic bombings of Hiroshima and Nagasaki. The studies mainly focused on fertility rather than measurements of the survivors' uteri. In one massive study of the reproductive history of around 24,000 people, Koseki data was utilized to determine fertility of the survivors. The study was limited to women married in 1945 that were of likely childbearing years. There was no significant difference in percent of live births between the different groups. Groups were based on distance from atomic bomb in both Hiroshima and Nagasaki. Interview questions included information on "abortions, sterilizations, use of contraceptives, attitudes toward family size, and the number and timing of products of conception" (Seigel 1966). It was noted that the conclusions from the study may be slightly inaccurate due to use of artificial abortions and contraceptives. Another study focused on the fertility of the survivors of Hiroshima and Nagasaki analyzed interviews of 2,345 women. It was discovered that the groups exposed to higher doses of radiation showed no loss of fertility compared to the those exposed to less radiation. The study also looked at the rate of conception in those that had used contraception at some point after the war compared to those that never used contraception. Interestingly, there was actually a higher birth rate in the women who had at some point used contraception compared to those who never used contraception following the bombings. When comparing the reproductive success of couples in Hiroshima and Nagasaki it was found that couples in Hiroshima aged 35-39 struggled the most as 60% failed to conceive following August 1945. The study overall concluded "no large long-range alterations in average fertility can be attributable to exposure to atomic radiation in 1945" (Blot 1972).

Radiation can cause deleterious effects on the body through the formation of reactive oxygen species (ROS), which act as proinflammatory mediators. In the body, ROS are produced as intermediates of metal catalyzed oxidation reactions, as byproducts of mitochondrial electron

transport, and by phagocytes as a normal defense against pathogens. Since ROS are products of normal cellular function, that can be beneficial intracellular and intercellular messengers acting on gene expression, signal cascades, and apoptosis. Regarding this study, ROS regulate the degradation of the endometrium. Elevated levels of ROS cause a pro-oxidative state that is generally harmful to the cell. Prolonged oxidative stress will cause the cell to leave the cell cycle and eventually undergo apoptosis. Reactive oxygen species can cause double stranded breaks in DNA which can cause mutations and cell death. Aerobic organisms such as humans and mice are highly susceptible to oxidative stress and have adapted mechanisms to neutralize ROS. For instance, there are antioxidant systems such as superoxide dismutase (SOD) and glutathione peroxidase (GPX). Super oxide dismutase catalyzes the conversions of two superoxide anions into hydrogen peroxide and oxygen. Following SOD, the enzyme catalase will convert hydrogen peroxide into water and oxygen, fully rendering the ROS into safe molecules (Suman et al 2013). Glutathione peroxidase is used clinically to determine oxidative stress by monitoring the ratio of its oxidized form to its reduced form.

Regarding inflamed tissues, NADPH Oxidase 2 (NOX 2) is considered the main producer of ROS since it reduces oxygen to superoxide. NOX 2 is an enzyme which induces the phagocyte to release ROS to destroy foreign pathogens. People with mutations in their NOX 2 gene often have chronic granulomatous disease which is characterized by serious recurring infections. ROS derived from NOX 2 has been shown to have a regulatory role in autoimmune disorders (Sareila et al 2011). To study the effects of inactivating the NOX 2 gene, NOX 2 knock out mice were used as well as mice treated with apocynin. Apocynin is a highly selective inhibitor of the NADPH Oxidase family and is known to reduce ROS levels in mice (Jackman, 2009). Furthermore,

apocynin is useful in radiation studies since it is a NADPH Oxidase inhibitor that does not interfere with normal immune cell functions except for prohibiting the release of ROS.

Hypothesis

The mice in this study were subjected to proton radiation since the “Radiation environment in outer space, compared to earth, mostly consists of high energy protons” (Suman et al, 2013).

We expect that mice that underwent the most radiation to have the thinnest myometrial layers. Furthermore, the apocynin-fed mice as well as the NOX-2 knockout mice should receive a protective effect from the deleterious ROS that will result in a thicker myometrial layer when compared to the wild type mice that were exposed to the same radiation dose.

Materials & Methods

Animals

Mouse reproductive tissue was received from the laboratories of Dr. Xiao Wen “Vivien” Mao and Dr. Michael Peacut from Loma Linda University in Loma-Linda, California. The mice involved in this study were purchased from Jackson Laboratory. The experiment utilized 36 C57BL/6 mice and 18 B6.129S6Cybb^{tm1Din/J} NOX2 knockout mice. C57BL/6 mice are the most common strain used in laboratories. B6.129S6Cybb^{tm1Din/J} NOX2 knockout mice are mice that lack NADPH Oxidase 2. Prior to experimentation the mice were acclimated to their environment under the following conditions: housed three to a cage, 12-hour day/night cycle, 68° F. The mice were fed a commercial pellet chow and hydrogel ad libitum.

After a week of adjusting to the new surroundings the mice were assigned to treatment groups and subgroups:

Designated Animal Treatment Groups & Subgroups Key		
Groups	Animal Subgroups	Treatment
Wildtype	A	Wildtype (WT) Control
	B	WT + 0.5Gy
	C	WT + 2.0Gy
Apocynin Fed	D	WT + 0Gy + Apocynin (Apo)
	E	WT + 0.5Gy + Apo
	F	WT + 2.0Gy + Apo
NOX2 Knockout	G	Knockout (KO) Control
	H	KO + 0.5Gy
	I	KO + 2.0Gy

Table 1. Designated Animal Treatment Groups & Subgroups Key.

The subgroups fall under three main treatment groups: wildtype, apocynin fed, and NOX2 knockout. The experiment was approved through the Institutional Animal Care and Use Committee of Loma Linda University.

Radiation Studies

The different proton radiation doses used in this study were 0Gy, 0.5Gy, and 2.0Gy. A gray can be defined as one joule of radiation energy per kilogram of matter. The mice received full body proton radiation at the Loma Linda Medical Center in the James M. Slater, M.D. Proton Treatment and Research Center. Radiation exposure duration was 10 minutes. For the 10-minute procedure the mice were placed in aerated 30mm x 30mm x 60mm boxes. The mice were subjected to 250 megaelectron volts (MeV) protons at an approximate dose rate of 0.7Gy/minute without anesthesia. Apocynin treated mice 0.6 mg/ml of apocynin in their drinking water a day before irradiation and seven days following the procedure.

Tissue Acquisition

Mice were sacrificed seven days following irradiation using carbon dioxide and vaginal smears were performed to determine the stage of the estrous cycle. The uteri were harvested within the hour and placed in a 4% paraformaldehyde solution for preservation and delivery to the laboratory of Dr. Forsman at East Tennessee State University. Prior to utilization of the uteri, the fat surrounding the tissues was trimmed and the weight of the uterine horns, uterine tubes, and ovaries were measured and recorded. The reproductive organs were then transferred to 70% ethanol until use.

Slide Preparation

The uterine horns were dehydrated and embedded using standard histological embedding techniques (Appendix A) with care being taken to orient the tissue vertically. Vertical orientation was necessary to ensure that cross sections through the uterine horn could be obtained. Tissues were sectioned at 4 μ m thickness using a microtome. The cross sections were mounted on glass slides with three sections of tissue for each animal on each slide. The slides were stained using hematoxylin and eosin following the standard H&E staining procedures. (Appendix B).

Image Acquisition

Stained tissue was viewed using a Zeiss Axioskop 40 microscope at 5x power and photographed with a Canon Powershot A640 camera. Measurements were obtained using the Carl Zeiss AxioVision software, version 4.7.0. Three images were taken per animal resulting in 147 images for analysis. Initially, 54 mice were in the study, but, only 49 uteri produced quantifiable images. Moreover, some of the tissues analyzed were used were in a previous study which focused on mucins and therefore were stained using Acian blue/periodic acid-Schiff stain.

In order to make accurate and unbiased measurements of the layers of the myometrium, a random number generator was used as well as a numbered grid superimposed over the tissue to determine where on the picture to measure. It should be noted that the rater was blinded to animal group during image acquisition. Fifteen measurements of the myometrial thickness were taken for each cross section: five of the outer longitudinal layer, 5 of the inner circular layer, and 5 of the total thickness of both layers.

Statistical Analysis

Two methods of calculating the total average thickness of the myometrial layers of the different treatment groups and subgroups were employed. The first took all the measurements from one animal subgroup (i.e. A1-A6) and averaged each layer's thickness. The second, averaged each individual animal's measurements and took the average of all of them. There was virtually no difference in the averages derived by either method.

One-way ANOVAs were conducted using the averages from the first method to analyze the effect of whole-body proton radiation on the thickness of the myometrial layers in the wildtype, NOX2 Knockout, and apocynin fed mice. To protect the integrity of the data, treatment groups the samples belonged to were left unknown until the statistical analysis.

Results

Data for the thickness of the individual and combined myometrial layers was collected for all treatment groups using the available animal tissue samples. A photomicrograph highlighting the different myometrial tissue layers is shown in Figure 1.

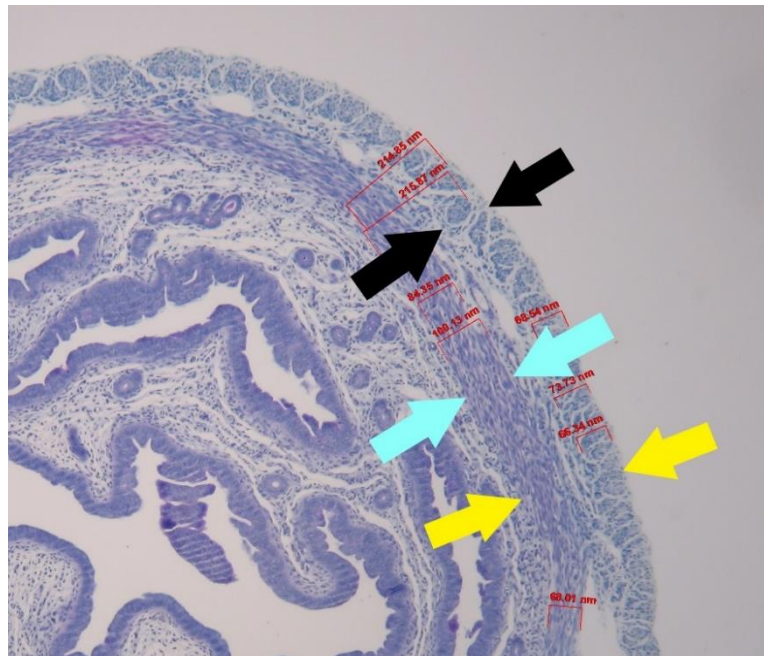


Figure 1. Cross section of the uterus depicting the outer longitudinal and inner circular layers of the myometrium with thickness measurements (50x). The arrows indicate the different layers and where they were measured: the black arrows indicate the outer longitudinal layer, the light blue arrows indicate the inner circular layer, and the yellow arrows indicate both layers.

Table 2 depicts the p-values calculated from the wildtype group's subgroup comparisons of the outer, inner, and both layers of the myometrium using an ANOVA. The outer myometrial layer pairings showed a statistically significant difference between the WT + 2.0Gy subgroup and the WT control subgroup ($p=0.005$). There was also a significant difference between the WT + 2.0Gy and the WT + 0.5Gy mice ($p=0$). The differences in the average thickness of the outer longitudinal layer of muscle is represented in Figure 2. The outer layer of WT + 2.0Gy subgroup had the thickest outer layer. The wildtype control and WT + 0.5Gy subgroups did not show a

statistical difference in the outer layer thickness ($p=0.766$). As for the inner layer, there was no statistical difference between any of the wildtype subgroups; therefore, an interval plot was omitted. The one-way ANOVA showed that there was a statistical difference between the WT + 2.0Gy subgroup and the other two subgroups for thickness of both layers ($p=0$, $p=0$). There was no statistical difference between the wildtype control and WT + 0.5Gy subgroups for both layers ($p=0.979$). In an interval plot, Figure 3 exhibits the difference in thickness of both myometrial layers. An example photomicrograph of each wildtype group subgroup can be found in Figures 4, 5, and 6.

One-Way ANOVA Comparison of Wildtype (WT) Subgroups	
Comparison Pairing	p- Value
Outer 0.5Gy vs. Outer Control	0.766
Outer 2.0Gy vs. Outer Control	0.005*
Outer 2.0Gy vs. Outer 0.5Gy	0*
Inner 0.5Gy vs. Inner Control	0.779
Inner 2.0Gy vs. Inner Control	0.204
Inner 2.0Gy vs. Inner 0.5Gy	0.508
Both 0.5Gy vs. Both Control	0.979
Both 2.0Gy vs. Both Control	0*
Both 2.0Gy vs. Both 0.5Gy	0*

Table 2. One-Way ANOVA Comparison of Wildtype (WT) Subgroups. WT Control vs. WT. + 0.5Gy vs. WT + 2.0Gy. P-values below the Value of Significance, $p=0.05$ are asterisked.

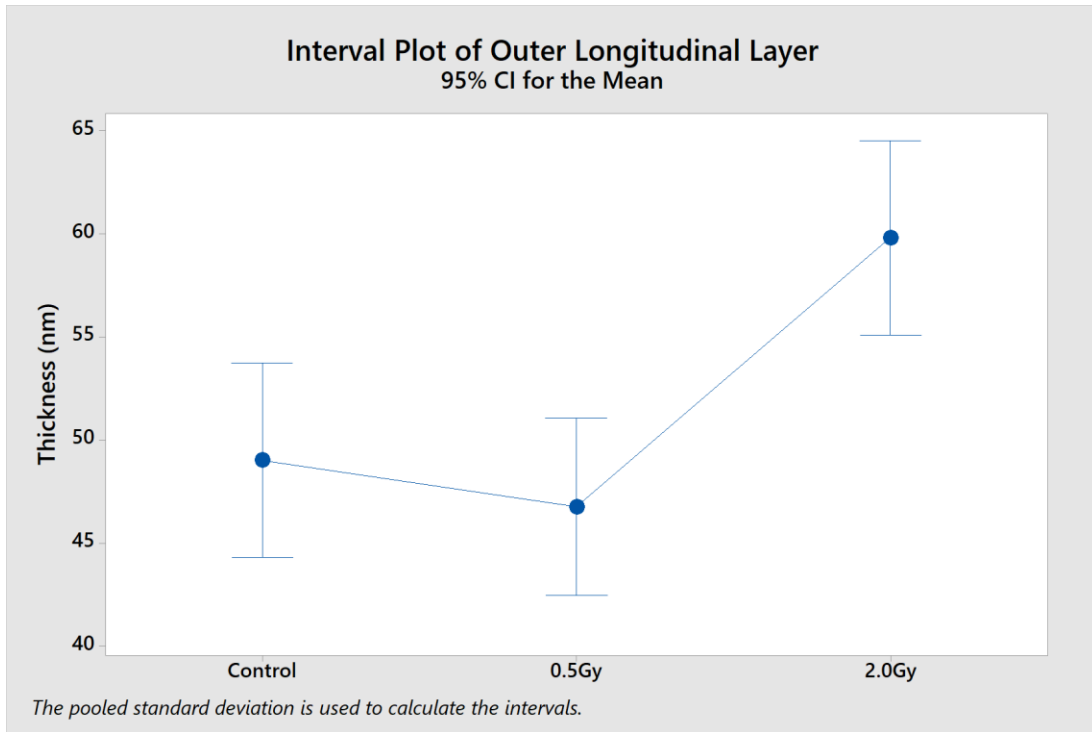


Figure 2. Interval Plot of Outer Thickness Layers of Wildtype (WT) Control (N=5), WT + 0.5Gy (N=6), and WT + 2.0Gy (N=5).

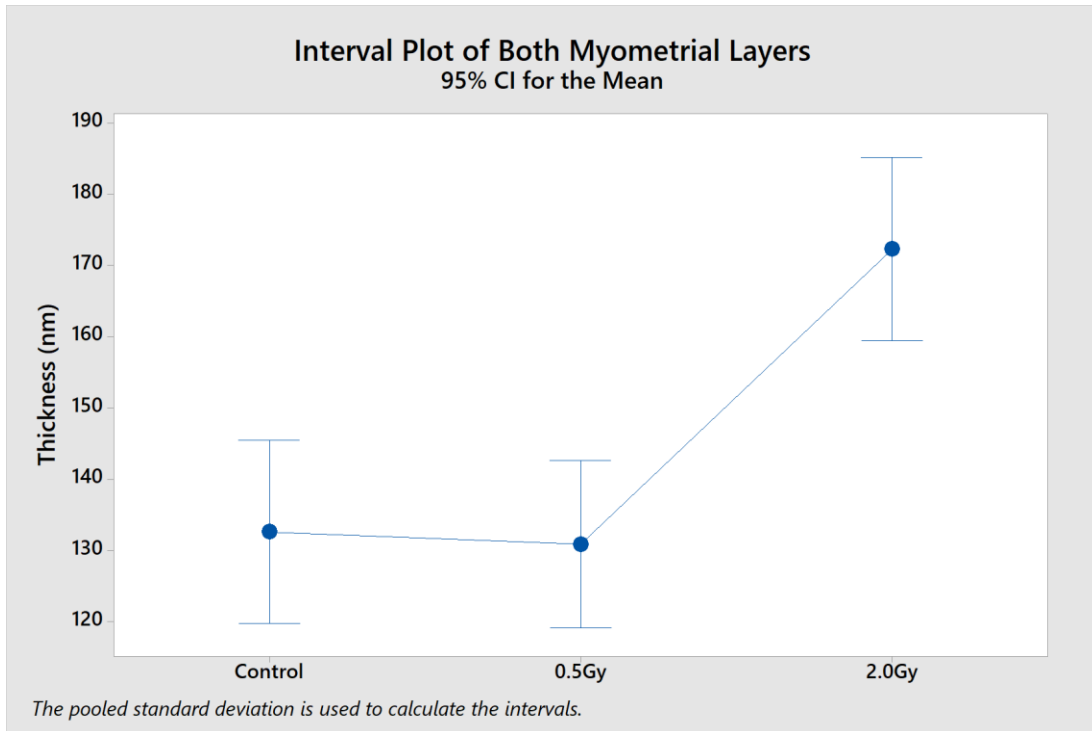


Figure 3. Interval Plot of Both Layers of Wildtype (WT) Control (N=5), WT + 0.5Gy (N=6), and WT + 2.0Gy (N=5).

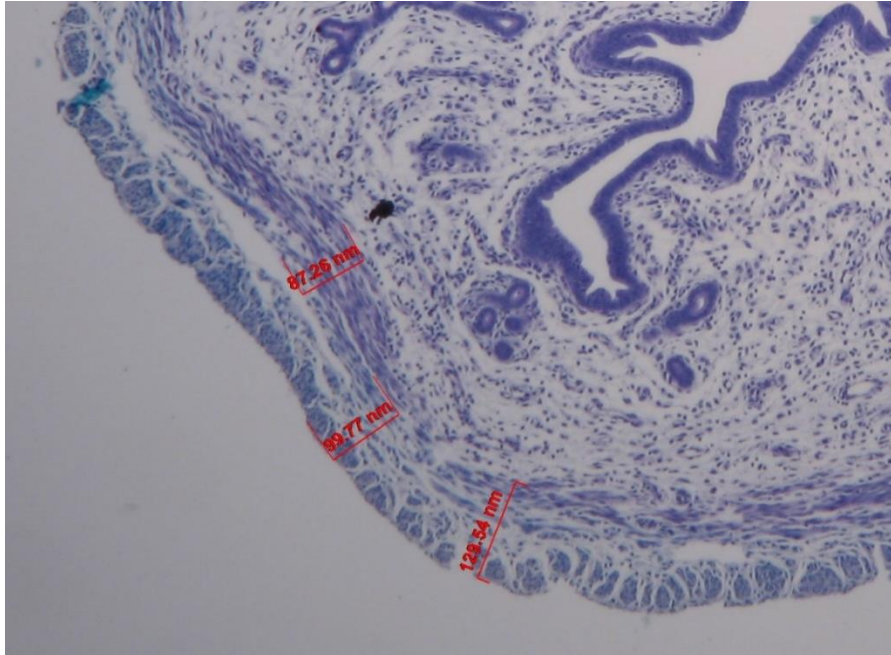


Figure 4. Cross section of the uterus from an animal belonging to subgroup A; Wildtype (WT) Control (50x).

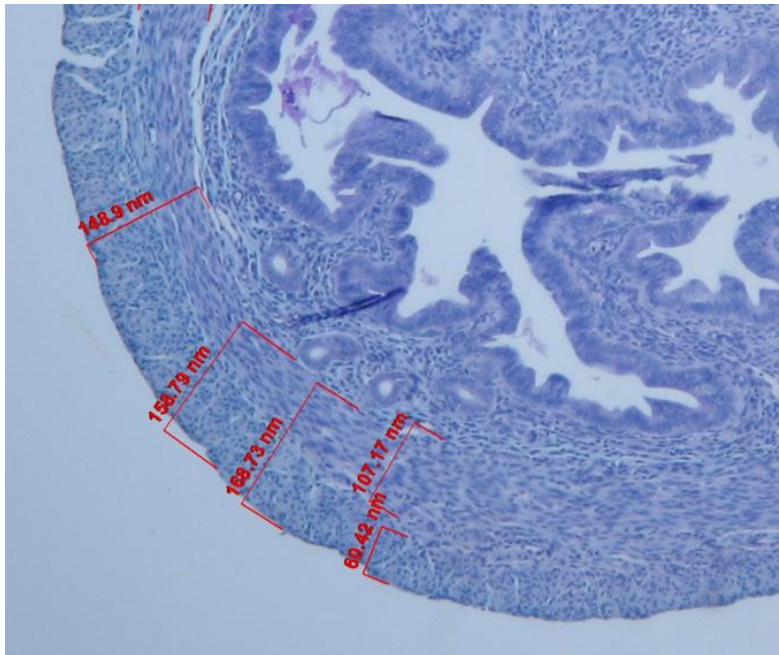


Figure 5. Cross section of the uterus from an animal belonging to subgroup B; WT + 0.5Gy (50x).

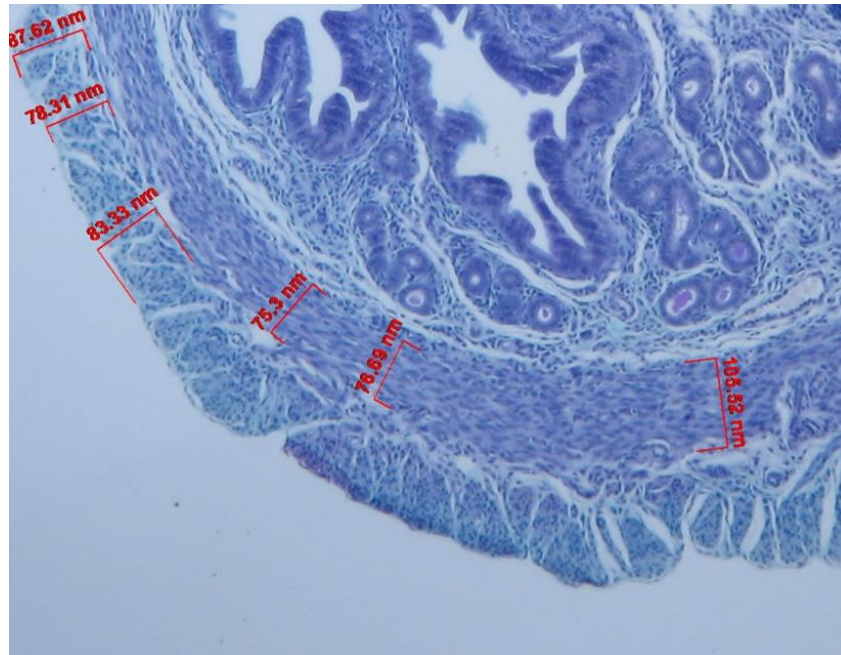


Figure 6. Cross section of the uterus from an animal belonging to subgroup C; WT + 2.0Gy (50x).

The P-values from the subgroup comparisons within the apocynin fed treatment group can be found in Table 3. The only statistical difference found amongst the outer longitudinal layer comparison was between WT + 0Gy + Apocynin and WT + 2.0Gy + Apo subgroups ($p=0.004$). Figure 7 depicts the difference of outer longitudinal layer thickness in an interval plot. The thickest layer was the WT + 0Gy + Apocynin subgroup. Amongst the inner circular layers, there was a statistical difference between the WT + 2.0Gy + Apo and the WT + 0.5Gy + Apo subgroups ($p=0.001$). An interval plot illustrating this can be seen in Figure 8. There was no statistical difference between WT + 0Gy + Apocynin ($N=6$) compared to both WT + 0.5Gy + Apo ($p=0.065$, $N=6$) and WT + 2.0Gy + Apo subgroups ($p=0.349$, $N=6$). The thickest layer is the WT + 0.5Gy + Apo subgroup. For both layers, there is a statistical difference between subgroup WT + 0Gy + Apocynin and subgroup WT + 2.0Gy + Apo ($p=0.04$). Presented as an interval plot, Figure 9 illustrates the statistical difference of the thickness of both myometrial layers. There is no statistical difference between subgroup WT + 0.5Gy + Apo and both WT + 0Gy + Apo and WT + 2.0Gy +

Apo subgroups ($p=0.955$, $p=0.081$). The thinnest layer was from the WT + 2.0Gy + Apo. Figures 11, 12, and 13 represent subgroups WT + 0Gy + Apo, WT + 0.5Gy + Apo, and WT + 2.0Gy + Apo respectively.

One-Way ANOVA Comparison of Wildtype (WT) + Apocynin Subgroups	
Comparison Pairing	p-Value
Outer 0.5Gy vs. Outer Control	0.132
Outer 2.0Gy vs. Outer Control	0.004*
Outer 2.0Gy vs. Outer 0.5Gy	0.396
Inner 0.5Gy vs. Inner Control	0.065
Inner 2.0Gy vs. Inner Control	0.349
Inner 2.0Gy vs. Inner 0.5Gy	0.001*
Both 0.5Gy vs. Both Control	0.955
Both 2.0Gy vs. Both Control	0.04*
Both 2.0Gy vs. Both 0.5Gy	0.081

Table 3. One-Way ANOVA Comparison of Wildtype (WT) + Apocynin Subgroups. WT + 0Gy + Apocynin vs. WT 0.5Gy + Apocynin vs. WT 2.0Gy + Apocynin. P-values below the Value of Significance, $p=0.05$ are asterisked.

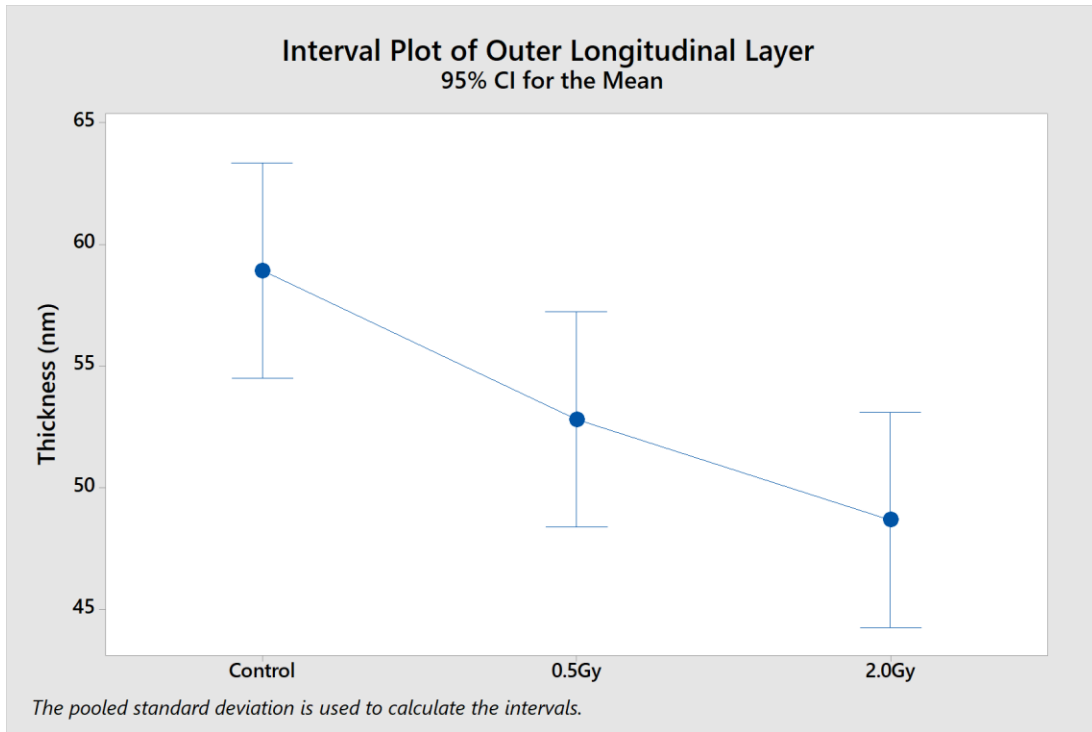


Figure 7. Interval Plot of Outer Layers of Wildtype (WT) + Apocynin (Apo) (N=6), WT + 0.5Gy + Apo (N=6), and WT + 2.0Gy + Apo (N=6).

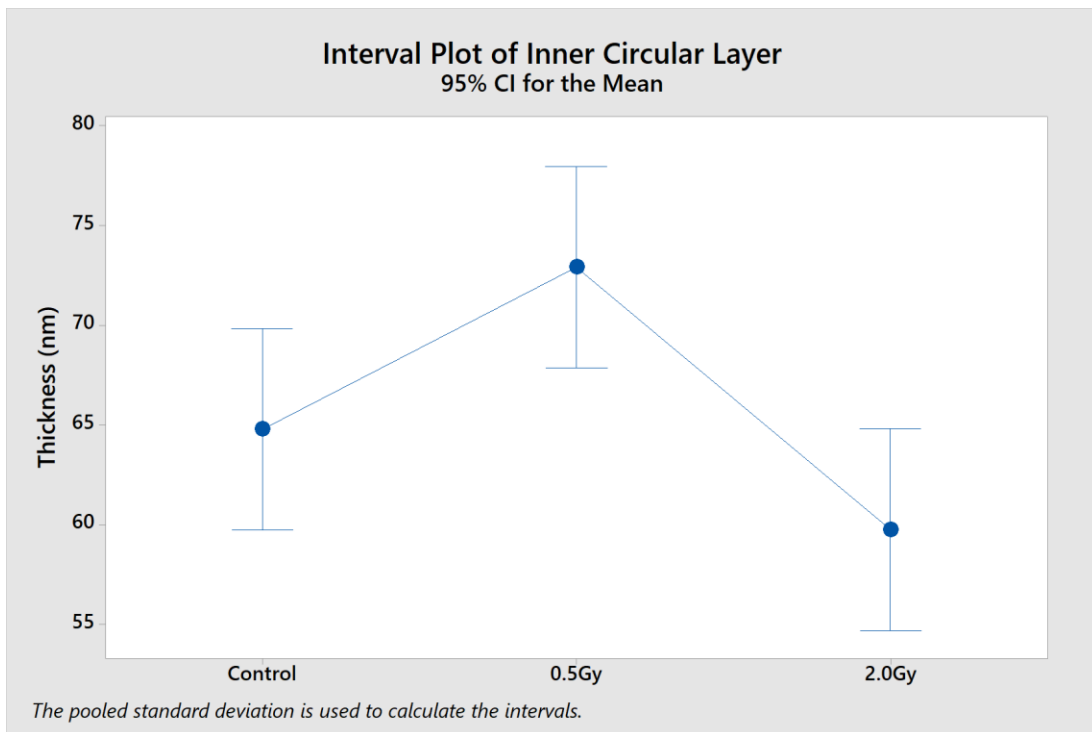


Figure 8. Figure 9. Interval Plot of Inner Layers of Wildtype (WT) + Apocynin (Apo) (N=6), WT + 0.5Gy + Apo (N=6), and WT + 2.0Gy + Apo (N=6). Thickness displayed on y-axis in nanometers.

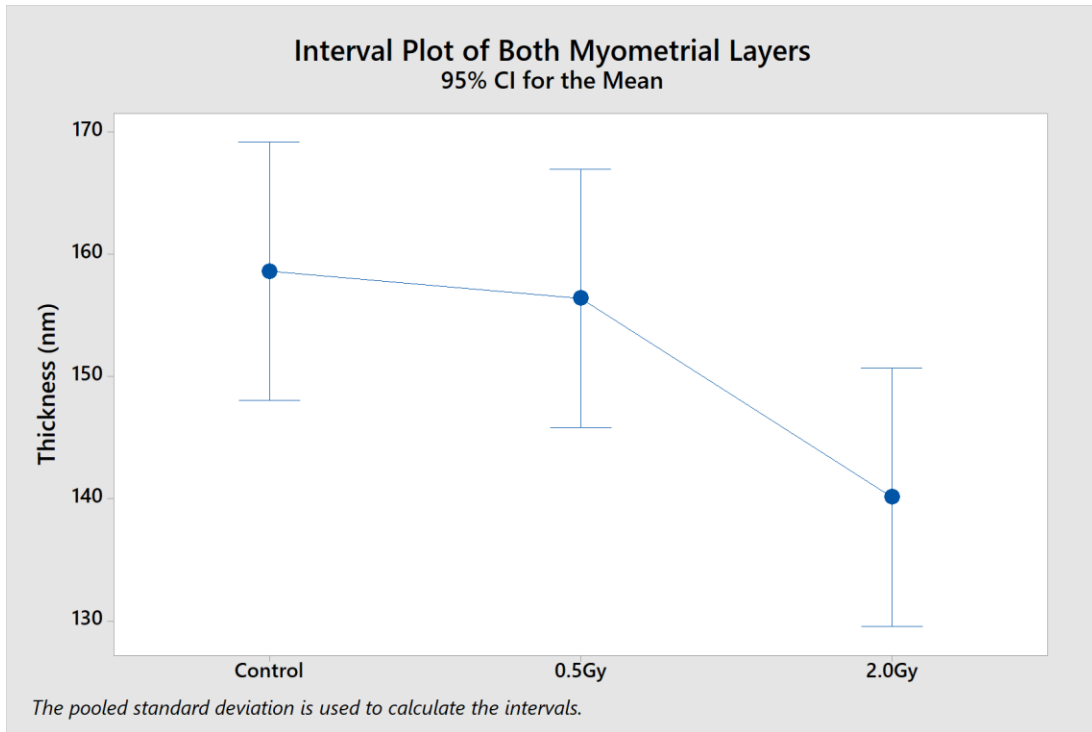


Figure 10. Interval Plot of Both Layers of Wildtype (WT) + Apocynin (Apo) (N=6), WT + 0.5Gy + Apo (N=6), and WT + 2.0Gy + Apo (N=6). Thickness displayed on y-axis in nanometers.

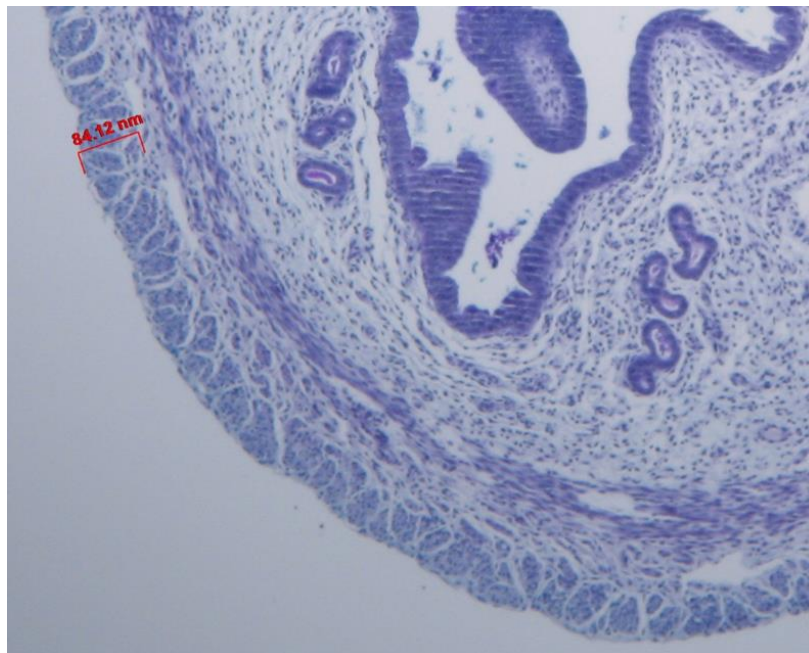


Figure 11. Cross section of the uterus from an animal belonging to subgroup D; Wildtype + Apocynin (Apo) (50x).

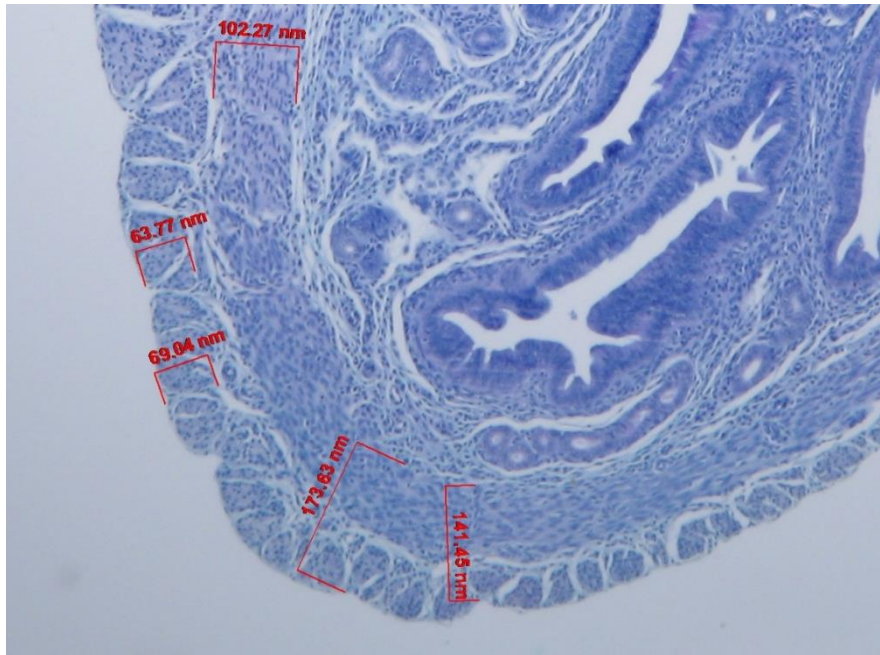


Figure 12. Cross section of the uterus from an animal belonging to subgroup E; WT + 0.5Gy + Apo (50x).

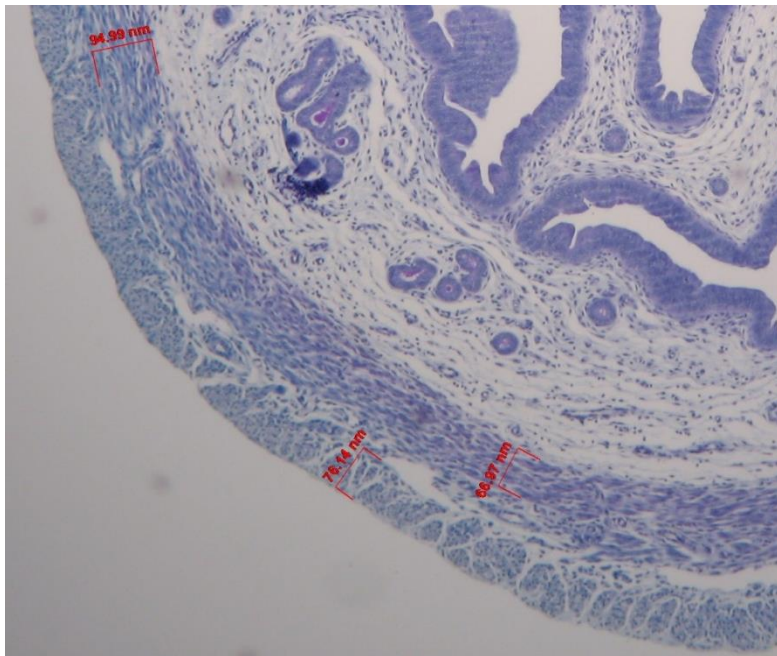


Figure 13. Cross section of the uterus from an animal belonging to subgroup F; WT + 2.0Gy + Apo (50x).

The statistical values or p-values from the knockout mice subgroup comparisons are shown in Table 4. There is a statistical difference between the knockout control subgroup and both

subgroups, KO + 0.5Gy ($p=0.045$, $N=4$) and KO + 2.0Gy ($p=0.001$, $N=6$) for the thickness of the outer longitudinal layer. The interval plot in Figure 14 clearly demonstrates the difference in thickness. The outer layer thickness of KO + 0.5Gy subgroup versus the KO + 2.0Gy subgroup is not statistically different ($p=0.612$). The thickest outer layer belongs to the knockout control subgroup. The inner layer only shows a statistical difference between the knockout control subgroup and the KO + 2.0Gy subgroup ($p=0.021$). Figure 15 shows the statistical difference in an interval plot. There is no statistical difference between subgroup KO + 0.5Gy and both the knockout control subgroup and KO + 2.0Gy subgroup. The KO + 2.0Gy subgroup has the thinnest inner layer. For both layers, there is a statistical difference between the KO + 0.5Gy and KO + 2.0Gy subgroups ($p=0.043$), which can be seen in an interval plot in Figure 16. No statistical difference was found between the knockout control subgroup and the other two subgroups, KO + 0.5Gy and KO+ 2.0Gy ($p=0.487$, $p=0.39$). The thickest of both layers belongs to the KO + 0.5Gy subgroup. A microphotograph of the all the Knockout group subgroups can be found in Figures 17, 18, and 19.

One-Way ANOVA Comparison of Knockout (KO) Subgroups	
Comparison Group	p-Value
Outer 0.5Gy vs. Outer Control	0.045*
Outer 2.0Gy vs. Outer Control	0.001*
Outer 2.0Gy vs. Outer 0.5Gy	0.612
Inner 0.5Gy vs. Inner Control	0.946
Inner 2.0Gy vs. Inner Control	0.021*
Inner 2.0Gy vs. Inner 0.5Gy	0.074
Both 0.5Gy vs. Both Control	0.487
Both 2.0Gy vs. Both Control	0.39
Both 2.0Gy vs. Both 0.5Gy	0.043*

Table 4. One-Way ANOVA Comparison of Knockout (KO) Subgroups. Knockout (KO) Control vs. KO + 0.5Gy vs. KO + 2.0Gy. P-values below the Value of Significance, $p=0.05$ are asterisked.

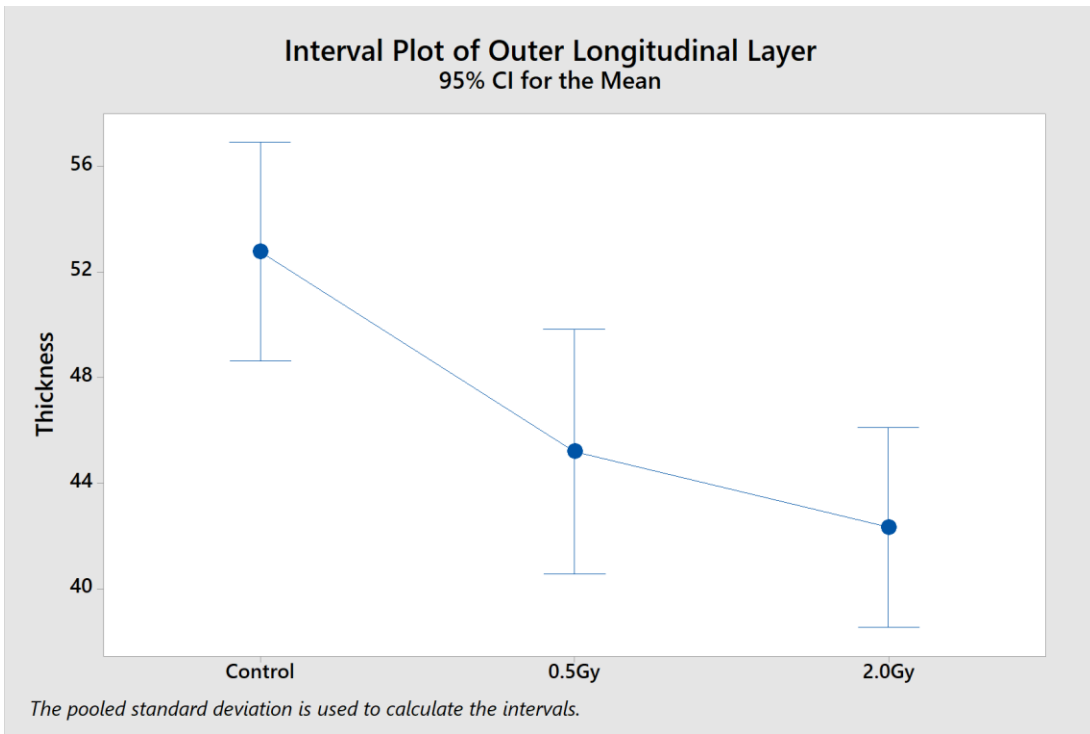


Figure 14. Interval Plot of Outer Layers of Knockout (KO) Control (N=5), KO + 0.5Gy (N=4), and KO + 2.0Gy (N=6).

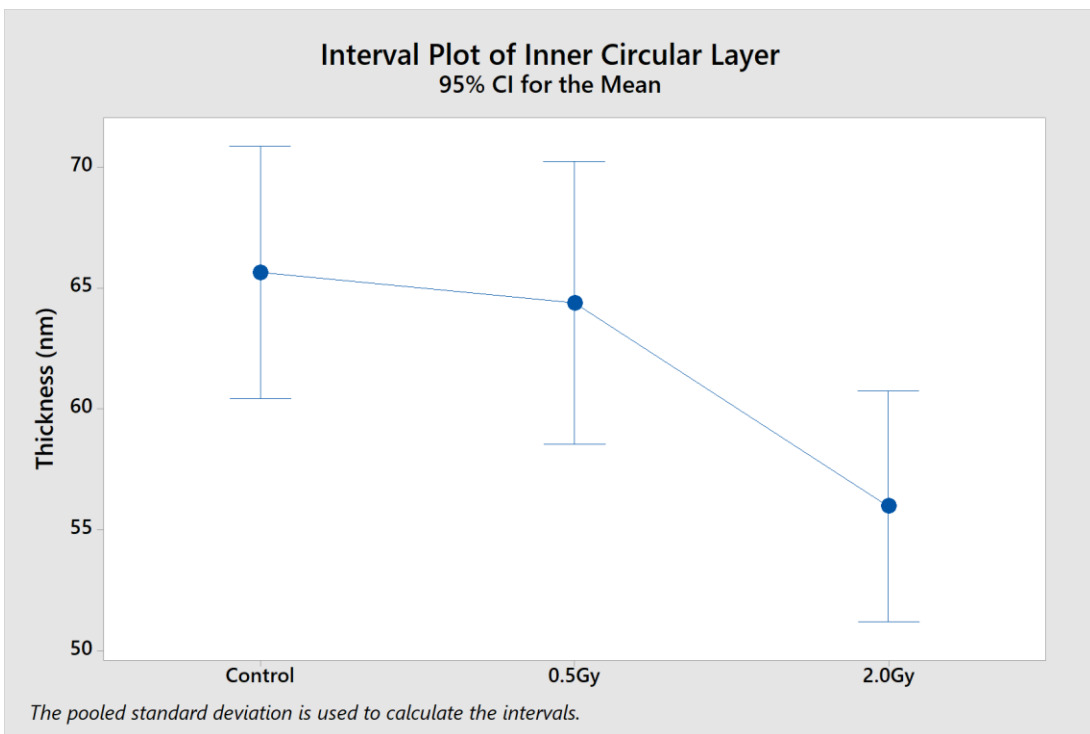


Figure 15. Interval Plot of Inner Layers of Knockout (KO) Control (N=5), KO + 0.5Gy (N=4), and KO + 2.0Gy (N=6).

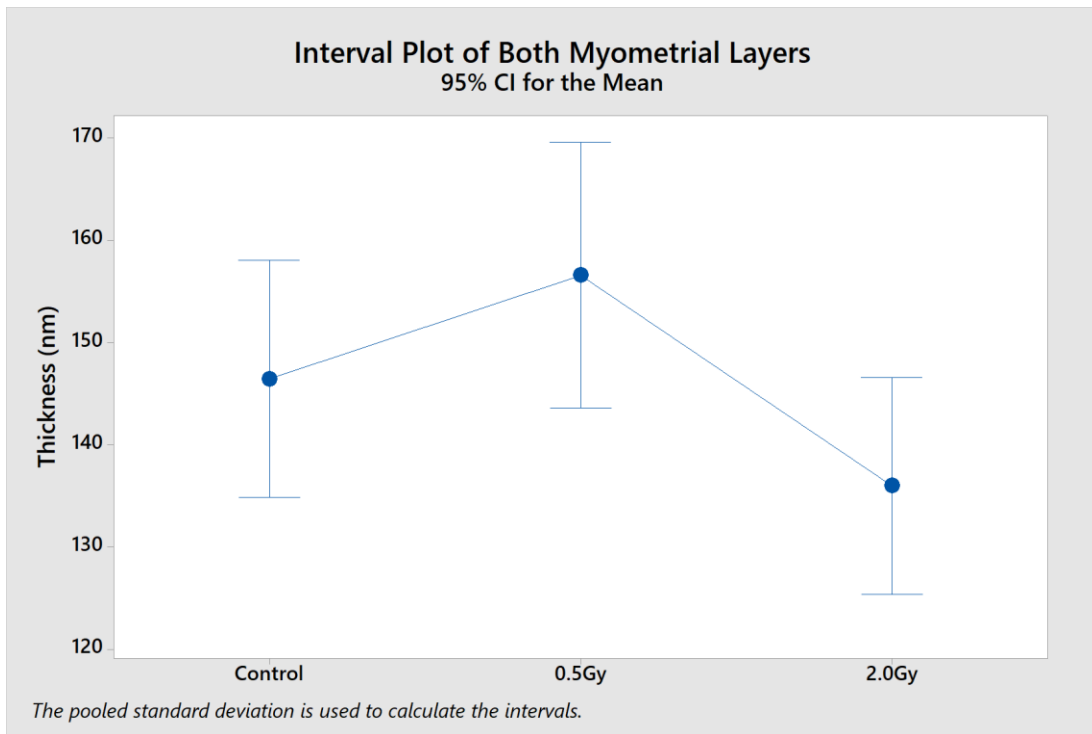


Figure 16. Interval Plot of Both Layers of Knockout (KO) Control (N=5), KO + 0.5Gy (N=4), and KO + 2.0Gy (N=6).

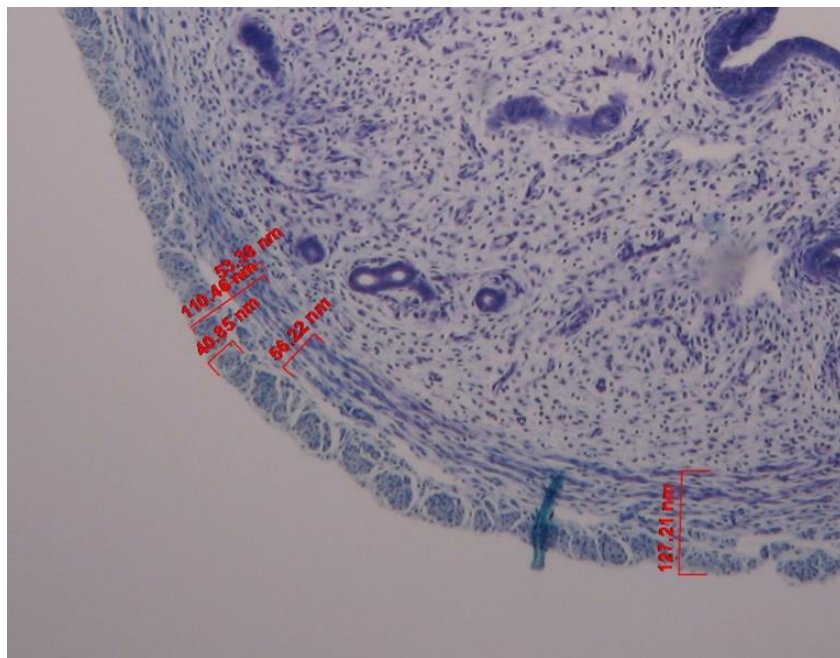


Figure 17. Cross section of the uterus from an animal belonging to subgroup G; Knockout (KO) Control (50x).

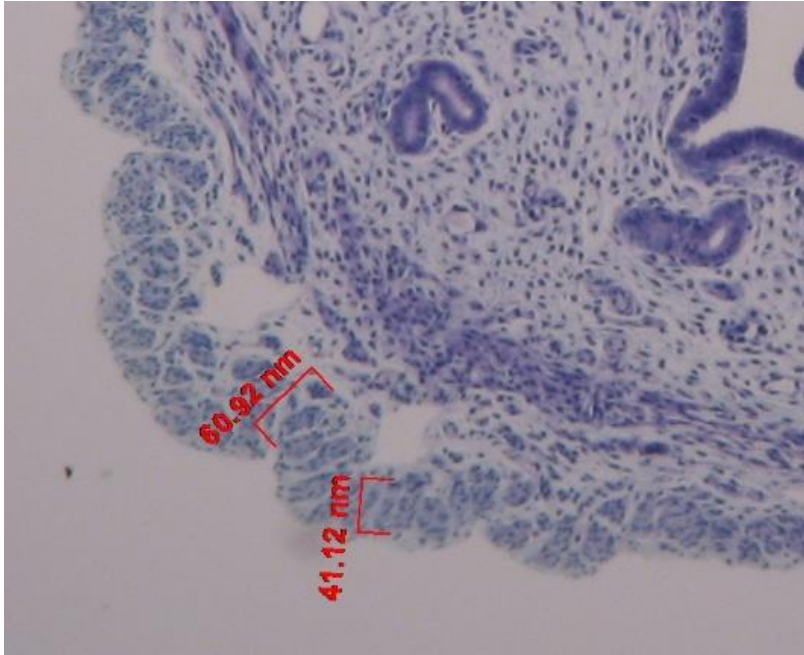


Figure 18. Cross section of the uterus from an animal belonging to subgroup H; KO + 0.5Gy (50x).

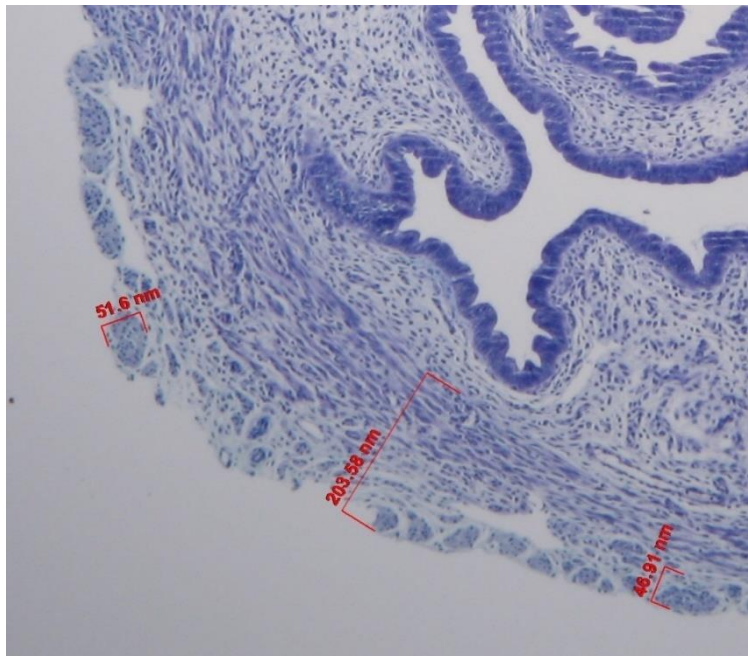


Figure 19. Cross section of the uterus from an animal belonging to subgroup I; KO + 2.0Gy (50x).

All the results between the wildtype control subgroup and WT+ Apocynin subgroup shown in Table 5 are statistically different except for the inner circular layer comparison ($p=0.632$). Since

the inner circular layer comparison shows no statistical difference an interval plotted was omitted. The outer longitudinal layer comparison of apo treated animals (N=6) to control animals (N=5) was statistically significant ($p=0.003$). Additionally, measurements that included both layers were statistically significant between wild type control mice and Apo-control mice ($p=0.001$, N=5,6). Figures 20 and 21 compile the data of the outer layer and both layers in an interval plot, respectively. For the outer and both layers, the WT + 0Gy + Apocynin subgroup was statistically thicker while the wildtype control subgroup was statistically thicker for the inner layer ($p=0.003$, $p=0.001$). An example of a cross section from the wildtype control subgroup can be found in Figure 4. Figure 11 depicts an example cross section of the WT + 0Gy + Apocynin subgroup.

One-Way ANOVA Comparison of Wildtype (WT) Control & Wildtype (WT) + Apocynin	
Comparison Pairing	p-Value
Outer WT + 0Gy + Apo Control vs. Outer WT Control	0.003*
Inner WT + 0Gy + Apo Control vs. Inner WT Control	0.632
Both WT + 0Gy + Apo Control vs. Both WT Control	0.001*

Table 5. One-Way ANOVA Comparison of Wildtype (WT) Control & Wildtype (WT) + Apocynin. WT Control vs. WT + 0Gy + Apocynin. P-values below the Value of Significance, $p=0.05$ are asterisked.

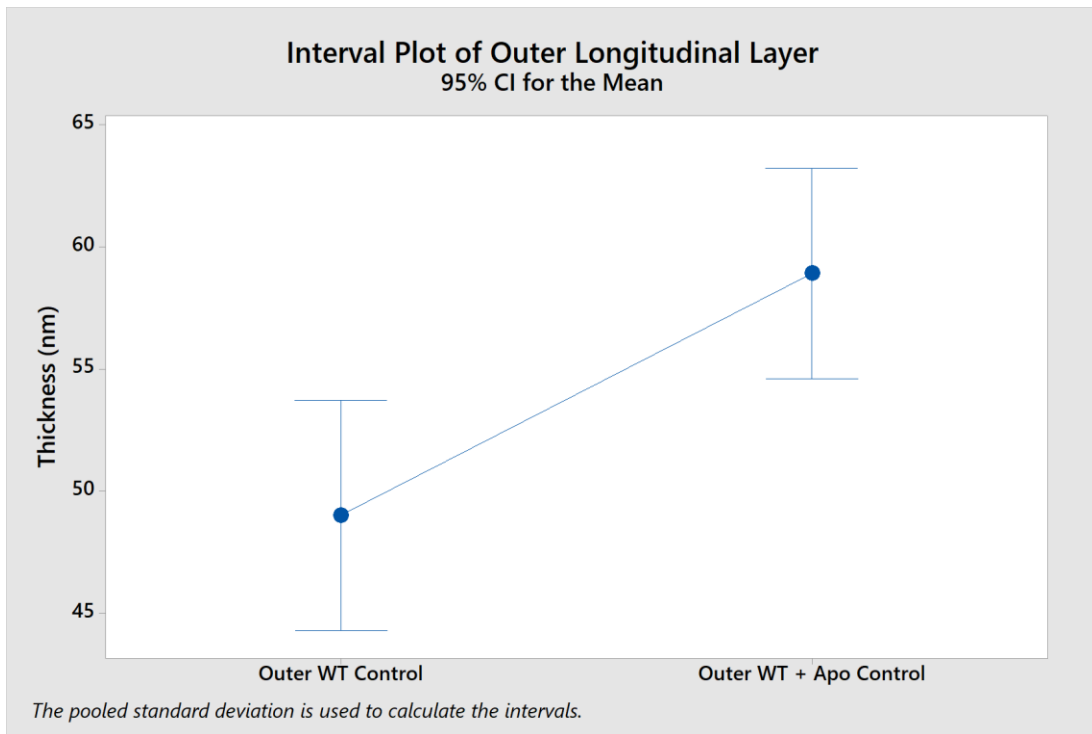


Figure 20. Interval Plot of Outer Layers of Wildtype (WT) Control (N=5) and WT + 0Gy + Apocynin (Apo)(N=6).

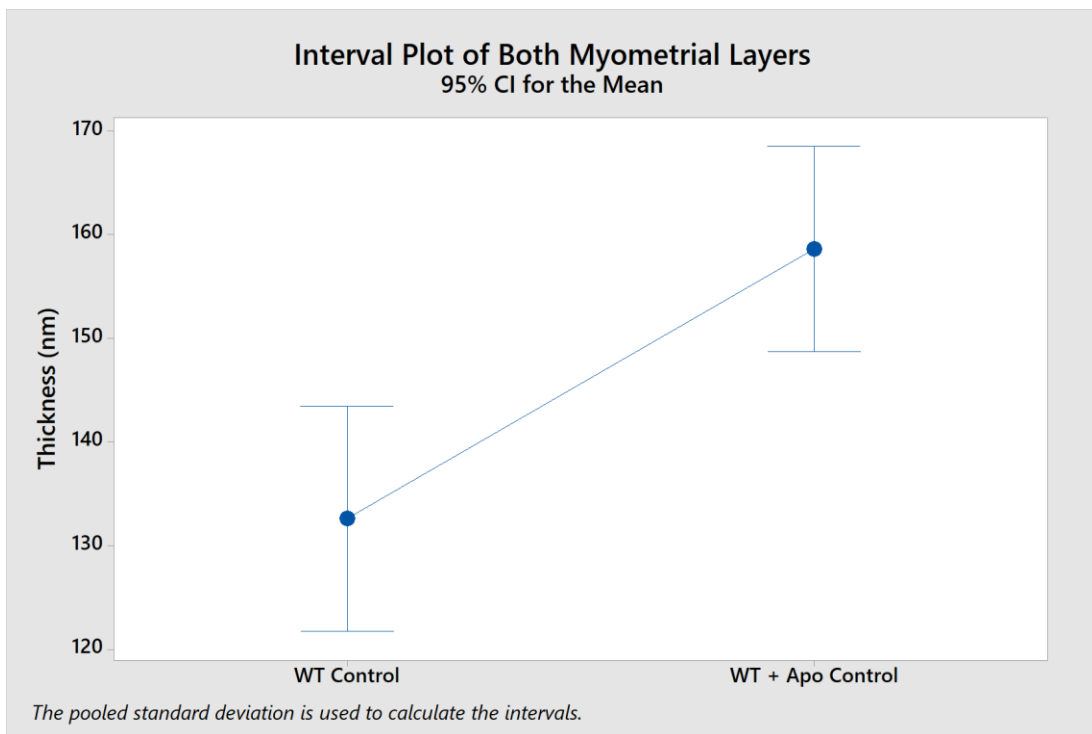


Figure 21. Interval Plot of Both Layers of Wildtype (WT) Control (N=5) and WT + 0Gy + Apocynin (Apo)(N=6).

None of the results shown in Table 6 were statistically different between the wildtype control subgroup and knockout control subgroup. Respectively, the outer, inner, and both layers had a p-value of 0.273, 0.818, and 0.1. The knockout control subgroup had the thicker outer and both layers while the wildtype control had the thicker inner layer.

One-Way ANOVA Comparison of Wildtype (WT) Control & Knockout (KO) Control	
Comparison Pairing	p-Value
Outer KO Control vs. Outer WT Control	0.273
Inner KO Control vs. Inner WT Control	0.818
Both KO Control vs. Both WT Control	0.1

Table 6. One-Way ANOVA Comparison of Wildtype (WT) Control & Knockout (KO) Control. WT Control vs. KO Control. P-values below the Value of Significance, $p=0.05$ are asterisked.

Although the female mice were housed together, the Lee Boot Effect was not witnessed.

Table 7 shows the various stages of estrous the mice were in before being euthanized.

Within-Group Estrous Phase Determination Counts, All Treatment Groups				
Treatment Group	Proestrus	Estrus	Metestrus	Diestrus
Wildtype (WT) Control	0	3	2	1
WT + 0.5Gy	0	4	1	1
WT + 2.0Gy	2	3	0	1
WT + 0Gy + Apocynin	2	2	0	1
WT + 0.5Gy + Apo	0	2	3	1
WT + 2.0Gy + Apo	1	1	4	0
Knockout (KO) Control	0	3	2	0
KO + 0.5Gy	0	2	1	1
KO + 2.0Gy	0	3	1	2
Totals	5	23	14	8

Table 7. Within-Group Estrous Phase Determination Counts, All Treatment Groups (Razskazovskiy, 2016).

Discussion

When evaluating the effect of radiation on the wildtype treatment group, each myometrial layer comparison showed that the WT + 2.0Gy subgroup had the thickest layers. We therefore reject our hypothesis that exposure to radiation would cause a thinning of the myometrial layers. Given that 2.0Gy is the highest level of radiation used, it was originally thought that the radiation would cause damaging ROS's to form and thin the layers of the myometrium.

As expected, the apocynin-fed treatment group comparisons showed that the outer longitudinal layer and combined layer measurements were statistically thickest for the WT + 0Gy + Apocynin subgroup. Given that the WT + 0gy + Apocynin subgroup received no radiation, it stands to reason that the inhibitory effects of apocynin reduced the damage from the ROS in the mice leading to thicker layers. Regarding the Knockout treatment, it was not surprising that the knockout control mice had the thickest outer longitudinal layer and both myometrial layers compared to the subgroups exposed to 0.5Gy and 2.0Gy. Overall, the study supported that the absence of NOX2 genes would lead to less ROS inside the mouse uterus to cause thinning of the myometrial layers.

Between the wildtype control subgroup and WT + 0Gy + Apocynin subgroup, the outer longitudinal layer and both layers measurements were thicker for the WT + 0Gy + Apocynin subgroup. This supports the hypothesis that the apocynin would provide an ameliorating effect to counteract the destructive nature of ROS. Although the wildtype control subgroup had thicker inner circular layers, no statistical difference was found using a one-way ANOVA. Comparing the wildtype control and the knockout control subgroups, there was no statistical difference in the thickness of any layer.

Limitations

The estrous phase of each mouse could be a confounding variable in the study. It was expected that all mice would experience the Lee Boot effect and be in diestrus as they were housed in an all-female setting and were not exposed to male urine (Whitten, 1959). Contrary to what was expected, only some of the female mice were found to be in the diestrus stage of the estrous cycle. Consequently, a confounding variable may have been introduced to the statistics of this study. In order to account for this, many disproportionate groups of each stage would need to be assigned from the nine subgroups already established. Moreover, there were not enough mice for the additional estrous cycle subgroups to have more than one animal assigned in all cases. Future studies should include a larger sample size of mice to account for effects from the estrous cycle in the event the Lee-Boot Effect is not witnessed.

Conclusion

The apocynin fed mice were statistically different in the thickness of their myometrial layers when compared within their own treatment group and against the wildtype control. The NOX2 Knockout treatment were only statistically different within the treatment group. There was no statistical difference when comparing the control mice of the wildtype group to the Knockout group. The results of this study suggest that the consumption of apocynin can reduce the deleterious effects of whole-body proton radiation by protecting the thickness of the myometrial layers. Future studies should include increasing sample size and ensure the female mice are all in diestrus.

References

- Baerwald, A. R., & Pierson, R. A. (2004). Endometrial development in association with ovarian follicular waves during the menstrual cycle. *Ultrasound in Obstetrics and Gynecology*, 24(4), 453–460. doi: 10.1002/uog.1123
- Boretto, M., Cox, B., & Noben, M. (n.d.). Development of organoids from mouse and human endometrium showing endometrial epithelium physiology and long-term expandability. *Human Development*, 1775–1786. doi: 10.1242/dev.148478
- Blot, W. J., & Sawada, H. (1972). Fertility among female survivors of the atomic bombs of Hiroshima and Nagasaki. *American journal of human genetics*, 24(6 Pt 1), 613–622.
- Caligioni C. S. (2009). Assessing reproductive status/stages in mice. *Current protocols in neuroscience, Appendix 4*, Appendix–4I. <https://doi.org/10.1002/0471142301.nsa04is48>
- Degani, S., Leibovitz, Z., Shapiro, I., Gonen, R., & Ohel, G. (1998). Myometrial thickness in pregnancy: longitudinal sonographic study. *Journal of Ultrasound in Medicine*, 17(10), 661–665. doi: 10.7863/jum.1998.17.10.661
- Demontis, G. C., Germani, M. M., Caiani, E. G., Barravecchia, I., Passino, C., & Angeloni, D. (2017). Human Pathophysiological Adaptations to the Space Environment. *Frontiers in physiology*, 8, 547. doi:10.3389/fphys.2017.00547
- Escalante NMM, Pino JH. Arrangement of muscle fibers in the myometrium of the human uterus: a mesoscopic study. *MOJ Anat Physiol*. 2017;4(2):280–283. DOI: [10.15406/mojap.2017.04.00131](https://doi.org/10.15406/mojap.2017.04.00131)

- Handlin, B. (2000). The Uterus: Changes in the Uterus during the Estrous Cycle. Retrieved April 1, 2020, from <https://instruction.cvhs.okstate.edu/Histology/fr/HiFRp14.htm>
- Hawkins, L., Robertson, D., Frecker, H., Berger, H., & Satkunaratnam, A. (2018). Spontaneous uterine rupture and surgical repair at 21 weeks gestation with progression to live birth: a case report. *BMC pregnancy and childbirth*, *18*(1), 132. doi:10.1186/s12884-018-1761-x
- Jackman, K., Miller, A., Silva, T. D., Crack, P., Drummond, G., & Sobey, C. (2009). Reduction of cerebral infarct volume by apocynin requires pretreatment and is absent in Nox2-deficient mice. *British Journal of Pharmacology*, *156*(4), 680–688. doi: 10.1111/j.1476-5381.2008.00073.x
- Ma, W., Miao, Z., & Novotny, M. V. (1998). Role of the Adrenal Gland and Adrenal-Mediated Chemosignals in Suppression of Estrus in the House Mouse: The Lee-Boot Effect Revisited1. *Biology of Reproduction*, *59*(6), 1317–1320. doi: 10.1095/biolreprod59.6.1317
- Norwitz, E. (2001). Placenta percreta and uterine rupture associated with prior whole body radiation therapy. *Obstetrics & Gynecology*, *98*(5), 929–931. doi: 10.1016/s0029-7844(01)01435-1
- Razskazovskiy, Vlad. (2016). The effects of proton irradiation on apical mucin thickness and acidity in the murine uterus. Thesis submitted to the ETSU Honors College, Spring 2016.
- Sareila, O., Kelkka, T., Pizzolla, A., Hultqvist, M., & Holmdahl, R. (2011). NOX2 Complex-Derived ROS as Immune Regulators. *Antioxidants & Redox Signaling*, *15*(8), 2197–2208. doi: 10.1089/ars.2010.3635

Seigel, D. G. (1966). Frequency of Live Births among Survivors of Hiroshima and Nagasaki Atomic Bombings. *Radiation Research*, 28(2), 278. doi: 10.2307/3572196

Suman, S., Rodriguez, O. C., Winters, T. A., Fornace, A. J., Albanese, C., & Datta, K. (2013). Therapeutic and space radiation exposure of mouse brain causes impaired DNA repair response and premature senescence by chronic oxidant production. *Aging*, 5(8), 607–622. doi: 10.18632/aging.100587

Wan Tinn Teh, Catharyn Stern, Sarat Chander, and Martha Hickey, “The Impact of Uterine Radiation on Subsequent Fertility and Pregnancy Outcomes,” *BioMed Research International*, vol. 2014, Article ID 482968, 8 pages, 2014. <https://doi.org/10.1155/2014/482968>.

Whitten, W.K. 1959. “Occurrence of anestrous in mice caged in groups. *Journal of Endocrinology*. 18: 102-107.

Appendix:**A. Tissue Embedding Process:**

Step 1: Turn on paraffin dispensing unit.

Step 2: Ensure all necessary materials are up to date and full: EtOH, Citrosolv, embedding mold release, etc.

Step 3: Procure the tissues to be embedded and label an identification tag for each using a pencil.

Step 4: Remove each individual tissue from its vial of 70% ethanol and place in an embedding cage along with its corresponding identification tag.

Step 5: In consecutive order at the appropriate times dehydrate/embed the tissues as follows:

80% EtOH: 30 minutes

90% EtOH: 30 minutes

95% EtOH: 30 minutes

100% EtOH: 30 minutes

100% EtOH: 30 minutes

50:50 100% EtOH: Citrosolv: 30 minutes

100% Citrosolv: 30 minutes

In the embedding oven

50:50 Hemo-De: Paraplast: 30 minutes

Paraplast 1: 1 hour

Paraplast 2: 1 hour

Step 6: While the tissues are being embedded, label the embedding rings with the appropriate tissue code.

Step 7: Immerse the embedding molds in mold release and allow to dry, then repeat.

Step 8: Place the embedding molds in the heated embedding mold chamber of embedding unit.

Step 9: With 15 minutes left in the 100% Citrosolv step turn on a hotplate.

Step 10: With 15 minutes left in the 50:50 Citrosolv/paraffin step turn on a second hotplate.

Step 11: With 5 minutes left in the Paraffin 2 step turn on the “cold plate”

Step 12: Individually, embed the tissues in paraffin and dissolve the excess paraffin in Citrosolv.

Step 13: Turn off the paraffin tank, embedding mold warming drawer, hotplates, and cold plate.

Step 14: Clean up.

B. Rehydration/Dehydration & Tissue Staining:

Take mounted tissue slides with appropriate identification written in pencil and place in dipping cage.

Step 1: In consecutive order at the appropriate times immerse the tissues as follows:

Hemo-de 1: 3 minutes

Hemo-de 2: 3 minutes

100% EtOH 1: 3 minutes

100% EtOH 2: 3 minutes

95% EtOH 1: 3 minutes

80% EtOH 1: 3 minutes

70% EtOH 1: 3 minutes

Distilled H₂O: 2 minutes

Distilled H₂O: 2 minutes

Distilled H₂O: 2 minutes

Tissue Staining:

Hematoxylin & Eosin Staining Technique

Step 1: Place slides in filtered hematoxylin for 3 minutes

Step 2: Rinse twice in distilled H₂O

Step 3: Run tap H₂O for five minutes

Step 4: Dip in acid alcohol 8-12 times

Step 5: Rinse twice in tap H₂O

Step 6: Rinse in distilled H₂O for a minute. Blot off excess H₂O.

Step 7: Dip in eosin for 30 seconds

Tissue Dehydration:

Step 4: In consecutive order at the appropriate times immerse the tissues as follows:

70% EtOH: 2 minutes

80% EtOH: 2 minutes

95% EtOH: 2 minutes

100% EtOH 3: 2 minutes

100% EtOH 4: 2 minutes

Hemo-de 3: 3 minutes

Hemo-de 4: 3 minutes

Step 5: Place a drop of permount on top of the tissue

Step 6: Carefully guide a cover slip on top of the permount and tissue while avoiding disturbing the tissue

Step 7: Let sit for 24 hours before viewing